The effect of rheumatoid arthritis and functional loading on the structure of the mandibular condyle in a transgenic mouse model: An FTIR study

Koletsi, Despina ; Eliades, Theodore ; Zinelis, Spiros ; Makou, Margarita ; Bourauel, Christoph ; Eliades, George

Abstract: OBJECTIVE: The objective of the present study was to investigate the effect of rheumatoid arthritis and functional loading through diet modification on the biochemical properties of the mandibular condyle in a transgenic mouse model and compare with healthy littermates. DESIGN: Twenty three, 4-week old hybrid male mice were used. Eleven were of transgenic line hTNF 197 (Tg 197 - with rheumatoid arthritis - RA) and 12 healthy littermates, both from mixed background CBAxC57BL/6. Four groups of mice were formed. Group 1 [n =5, RA-hard] included transgenic mice and received ordinary (hard) diet; group 2 [n=6, RA-soft] included transgenic line and received soft diet; group 3 [n=6, control-hard] were healthy littermates receiving ordinary (hard) diet and group 4 [n=6, control-soft] were healthy littermates with soft diet. Experimental period was 28 days. Following sacrifice, the mandibular condyles were subjected to micro-attenuated reflection Fourier transform infrared spectroscopy (micro-ATR FTIR) to reveal collagen/proteoglycan conformation of the condylar cartilage, while resin-embedded and metallographically polished specimens were evaluated through reflection FTIR microscopy to identify mineralization status of the corresponding condylar bone. RESULTS: The multivariable analysis revealed significantly lower a-helix to amide I percentage area ratio for the transgenic animals after adjusting for diet (=-4.29, 95% CIs: -8.52, -0.06; p=0.04). Mineral phase indices did not differ significantly between RA and control groups regardless the type of diet. CONCLUSIONS: Internal derangement of the anatomical structure with denaturation in the collagen structural components of the mandibular condyles of the RA animals was found, while no association with functional loading through diet modification was recorded.

DOI: https://doi.org/10.1016/j.archoralbio.2015.10.007

DOI: https://doi.org/10.1016/j.archoralbio.2015.10.007

The effect of rheumatoid arthritis and functional loading on the structure of the mandibular condyle in a transgenic mouse model: An FTIR study

Despina Koletsi[a], Theodore Eliades[b,*], Spiros Zinelis[c], Margarita Makou[d], Christoph Bourauel[e], and George Eliades[f]

[a] Endowed Chair of Oral Technology, School of Dentistry, University of Bonn, Welschnonnenstraβe 17, 53111 Bonn, Germany and Department of Orthodontics, School of Dentistry, University of Athens, Thivon 2, 11527 Goudi, Athens, Greece (d.koletsi@gmail.com)
[b] Clinic of Orthodontics and Paediatric Dentistry, Center of Dental medicine, University of Zurich, Plattenstrasse 11, CH-8032 Zurich, Switzerland (Theodore.Eliades@zzm.uzh.ch)
[c] Department of Dental Biomaterials, School of Dentistry, University of Athens, Thivon 2, 11527 Goudi, Athens, Greece (szinelis@dent.uoa.gr)
[d] Department of Orthodontics, School of Dentistry, University of Athens, Thivon 2, 11527 Goudi, Athens, Greece (mmakou@dent.uoa.gr)
[e] Endowed Chair of Oral Technology, School of Dentistry, University of Bonn, Welschnonnenstraβe 17, 53111 Bonn, Germany (bourauel@uni-bonn.de)
[f] Department of Dental Biomaterials, School of Dentistry, University of Athens, Thivon 2, 11527 Goudi, Athens, Greece (geliad@dent.uoa.gr)

Running Title: Arthritis and loading effect on condyle

***Corresponding author:** Theodore Eliades, Plattenstrasse 11, Zurich 8032, Switzerland, email Theodore.Eliades@zzm.uzh.ch

The effect of rheumatoid arthritis and functional loading on the structure of the mandibular condyle in a transgenic mouse model: An FTIR study

Structured abstract

Objective: The objective of the present study was to investigate the effect of rheumatoid arthritis and functional loading through diet modification on the biochemical properties of the mandibular condyle in a transgenic mouse model and compare with healthy littermates.

Design: Twenty three, 4-week old hybrid male mice were used. Eleven were of transgenic line hTNF 197 (Tg 197- with rheumatoid arthritis-RA) and 12 healthy littermates, both from mixed background CBAxC57BL/6. Four groups of mice were formed. Group 1 [n=5, RA-hard] included transgenic mice and received ordinary (hard) diet; group 2 [n=6, RA-soft] included transgenic line and received soft diet; group 3 [n=6, Control-hard] were healthy littermates receiving ordinary (hard) diet and group 4 [n=6, Control-soft] were healthy littermates with soft diet. Experimental period was 28 days. Following sacrifice, the mandibular condyles were subjected to micro-attenuated reflection Fourier transform infrared spectroscopy (micro-ATR FTIR) to reveal collagen/proteoglycan conformation of the condylar cartilage, while resin-embedded and metallographically polished specimens were evaluated through reflection FTIR microscopy to identify mineralization status of the corresponding condylar bone.

Results: The multivariable analysis revealed significantly lower a-helix to amide I percentage area ratio for the transgenic animals after adjusting for diet (β=-4.29, 95%CIs: -8.52, -0.06; p=0.04). Mineral phase indices did not differ significantly between RA and control groups regardless the type of diet.

Conclusions: Internal derangement of the anatomical structure with denaturation in the collagen structural components of the mandibular condyles of the RA animals was found, while no association with functional loading through diet modification was recorded.

Keywords: mandibular condyle, rheumatoid arthritis, FTIR, biochemical, functional loading

1. Introduction

The mandibular condyle has been considered a key functional element in the stomatognathic system, in human, primates and other inferior animal species. The head of the condyle, consists of a fibrous connective tissue layer, superior to the thin cartilage layer that is constantly contributing differentiating chondrocytes into osteoblasts responsible for bone formation during growth.[1,2] The remainder of the tissue consists of subchondral/subcartilage bone which can be distinguished to the cortical envelope and the trabecular/ lamellar bone mass, representing the cancellous component.[3] The mandibular condyle acts as a fulcrum and allows the mandible to perform translational and rotational movements, during mastication.[4]

The range and intensity of masticatory loading may provoke macroscopic or microscopic alterations on the structural background of craniofacial bones.[5,6] Induced modifications in functional loading by softening the ingredients of daily food consumption or suppression of biting capacity through the induction of constant disocclusion of teeth (trimming of incisors) have been well recognized as common epigenetic factors, contributing to reduced masticatory force levels being delivered to the temporomandibular joint (TMJ) and the mandibular condyles.[7-9]

Research in the direction of collagen disorders (rheumatoid arthritis, osteogenesis imperfecta, Ehlers-Danlos syndrome, Stickler syndrome, Marfan syndrome) has shed light on the involvement of genetic factors in the bone/cartilage architectural alterations.[10,11] Collagen represents the most abundant matrix protein, either as type I (bone) or type II (cartilage), and comprises three major polypeptide chains, resulting in fibril formation cross-linked to each other.[12] Defects in collagen synthesis have been linked to reduced cortical bone mineral density, altered orientation of collagen fibrils resulting in more fragile bones and higher risk for fractures.[13] More specifically, structural changes in the mandibular condyle, such as erosions and cyst formation, reduced thickness of

condylar cartilage, as well as decreased joint space, and flattening of the articular eminence and the condylar head and osteophytosis have been described in patients diagnosed with rheumatoid arthritis.[14-16] In addition, a number of studies have investigated the effects of functional loading, through physical exercise on bone structure alterations in particular within patients suffering from rheumatoid arthritis; available evidence from major joints (hip, spine) highlights the potential of long term, high intensity activity programs to decelerate mineral bone loss.[17,18] There is currently no evidence regarding the combined effect of functional loading and rheumatoid arthritis on the mandibular condyle.

Therefore, the aim of the present study was to investigate the effect of rheumatoid arthritis and functional loading through diet modification on the biochemical properties of the mandibular condylar cartilage and bone in a transgenic mouse model relative to healthy littermates. The null hypothesis is that there is no difference in structure characterization (collagen integrity of cartilage and bone mineralization) of the mandibular condyle of the diseased animal models receiving either hard or soft diet as compared to healthy animals subjected to the same diet.

2. Materials and Methods

2.1 Animals

Twenty three hybrid male mice were used. Eleven were of transgenic line hTNF 197 (Tg 197- with rheumatoid arthritis- RA) from mixed background CBAxC57BL/6 and the rest were healthy littermates CBAxC57BL/6. The sample was obtained from the Biomedical Sciences Research Center "Alexander Fleming" in Vari, Greece.[19] The study protocol was approved by the Veterinary Directorate and received the protocol number 1401/07-03-2014, with registration number EL BIO 005, according to the country's legislation (P.D 56/2013), conforming to the European Directive

2010/63/EU on the protection of vertebrate animals used in experimental and other scientific purposes.

Four groups of mice were formed. Group 1 [n=5, RA-hard] included transgenic (RA) mice receiving ordinary (hard) diet throughout the experimental period. Group 2 [n=6, RA-soft] included RA line receiving a soft diet. Group 3 [n=6, Control-hard] were healthy littermates receiving ordinary (hard) diet and Group 4 [n=6, Control-soft] again healthy littermates receiving a soft diet. The soft diet was produced by the same pellets used for the ordinary food after blending them with water in standardized proportions to achieve porridge like consistency.

The 28^{th} day of the animals' age was determined as day 1 of the experiment. During the experimental period all the animals were fed and watered *ad libitum* and their physiologic growth and development was closely monitored. Experimental living conditions followed National and European legislation and standards, including cages (Tecniplast S.P.A., Italy) and environment with 55% relative humidity, central ventilation (15 air changes/h), temperature of 20°C ± 2°C and artificial 12-h light-dark cycle. The total experimental period was set at 4 weeks. At the end of the experiment, the animals were sacrificed after being transiently anaesthetized in an ether chamber, the mandibles were separated from the heads and stored in 70% ethanol (right and left hemi-mandibles with the condyles separately).

2.2 Analysis of condylar cartilage

The left mandibular condyles were pressed against a single reflection diamond reflective element of a micro-attenuated total reflection accessory (Golden-Gate; Specac, USA) attached to a Fourier transform infrared spectrometer (Spectrum GX FTIR; Perkin-Elmer, UK). Spectra were recorded under the following conditions: Deuterated triglycine sulphate detector (DTGS), 4000-600 cm^{-1} range, 4 cm^{-1} resolution, 40 scans co-addition, 1 mm^2 sampling area, ZnSe lenses. The depth of

analysis was estimated as to 2 μm, therefore limiting the analysis to condylar cartilage. Spectra were subjected to baseline and ATR corrections, and then curve-fitted (Lorentz area mode), employing the 2nd derivative peak method (1750-1550 cm^{-1} and 1400-900 cm^{-1} regions) using Peak-Fit v4.12 software (SeaSolve Software, USA). The peak area ratios of the amide I secondary structure components relative to the entire amide I peak (1750-1550 cm^{-1}) were calculated to assess the collagen state. Likewise, the peak ratios of proteoglycans (PG) to amide I peaks (1400-900 cm^{-1}) were recorded, to allow for evaluation of the relative carbohydrate concentration of the condylar cartilage.

2.3 Analysis of condylar bone

The condylar specimens were further embedded in epoxy resin in a direction parallel to the longitudinal axis of the condyle. The specimens were ground with 600-4000 grit size silicon carbide papers under water cooling for 2 min each, polished with alumina suspensions (MD-Nap; Buehler, USA) up to 1 μm for 3 min, in a grinding/polishing machine (Ecomet III, Buehler), and cleaned in an ultrasonic water bath for 5 min. Spectra were acquired from the subchondral bone area employing an FTIR microscope (AutoImage; Perkin-Elmer) attached to the FTIR spectrometer under the following conditions: mercury cadmium telluride detector (MCT), 2000- 650 cm^{-1} wave number range, 4 cm^{-1} resolution, 200 μm X200 μm sampling window 128scans co-addition. All spectra were subjected to Kramers-Kroning transformation and baseline correction. The peak area ratios of the bone mineral component (PO_4 *v1,v3:* 1200-900 cm^{-1}) to bone organic matrix (C=O *v1* of R_1-CONH-R_2 -amide I: 1650 cm^{-1}) were used to calculate the mineral to matrix bone ratios (M). Moreover, the mineral region (1150-950 cm-1) was subjected to Gaussian curve deconvolution using the Peak-Fit v4.12 software to assess the acid phosphate content (peak area ratios of the acid phosphate

component at 1116 cm^{-1} vs the entire phosphate peak) and the crystallinity (peak area ratios of deconvoluted components at 1030 vs 1020 cm^{-1}).

2.4 Statistical analysis

Descriptive statistics were used to present the results of this study. Univariable and multivariable linear regression was performed, in order to assess the effects of the disease (rheumatoid arthritis) and type of loading (hard diet/soft diet) (predictor variables) on the outcomes of interest (a-helix to amide I, PG to amide I ratios for the condylar cartilage and mineral to matrix ratio, acid phosphate content and crystallinity for the condylar bone). Standard errors (SE) were calculated using the bootstrap method with 500 replications. The level of significance was pre-specified at a=0.05. All statistical analyses were conducted with STATA® version 12.1 software (Stata Corporation, College Station, Texas, USA).

3. Results

3.1 Analysis of condylar cartilage

Representative ATR-FTIR spectra from the condylar cartilage region for each testing group are illustrated in Figure 1. The peaks identified were assigned to COOH str (1740 cm^{-1}), amide I (C=O str of NHCO at 1650 cm^{-1}), amide II (N-H b and C-N str of NHCO at 1540 cm^{-1}), C=O str and CH3/CH2 b (1460-1410 cm^{-1}), amide III (C-N str and N-H b of NHCO at 1250 cm^{-1}), C=O b (1150 cm^{-1}), C-C str of polysaccharide ring (1100-1050 cm^{-1}), C-OH str (1050-1000 cm^{-1}), and C-O-S str (860 cm^{-1}), where str and b the stretching and bending vibrations respectively.

Deconvolution of amide I band (1700-1600 cm^{-1}) by peak fitting the second derivative spectra (Figure 2), revealed seven separate subpeaks associated with collagen secondary structure configurations, within the following regions: 1697-1695 cm^{-1} (turns), 1684-1682 cm^{-1} (β-sheets),

1671-1666 cm^{-1} (a-helix), 1650-1647 cm^{-1} (random coils), 1637-1631cm^{-1} (β-sheet), 1623-1620 cm^{-1} (unordered/unrecognized structure). Secondary peaks residing in lower frequencies than the original 1671-1666 cm^{-1} and within the a-helix region (1662-1660 cm^{-1}) were frequently identified in the control groups. Also, sporadically identified peaks were those of 1612-1606 cm^{-1} and 1601-1593 cm^{-1}.

Second derivative fitted spectra of amide III region (Figure 3) revealed characteristic subpeaks at 1287-1282 cm^{-1} (β-turns), 1264-1257 cm^{-1} (random coils/unordered structure), 1241-1234 cm^{-1} (β-sheets) and 1204-1200 cm^{-1} (S-O). Beta-sheets within the amide III region was the most prominent secondary structure identified in both RA and control specimens, whereas the band assigned to unordered structure at 1264-1257 cm^{-1} was absent in 1/3 of the control specimens.

Similarly, for the PG region, identifiable peaks were observed at 1085-1077 cm^{1}, 1048-1042 cm^{-1}, 1035-1025 cm^{-1} and 1016-1010 cm^{-1}, all related to carbohydrate vibration bands and resulting from pyranose ring vibrations; the first were assigned to C-C stretching vibrations of the polysaccharide ring, while the rest to C-OH stretching vibrations. Secondary peaks at 1064-1059 cm^{-1} related to polysaccharide ring vibrations were scarcely observed both in RA (n=2) and control groups (n=3).

The results of the descriptive statistics for a-helix (1671-1660cm^{-1}) to amide I and PG to amide I ratios are presented in Table 1. The percentage peak area ratio of a-helix (combined areas of 1671-1666 cm^{-1} and 1662-1660 cm^{-1}) to the entire amide I peak area was significantly lower for the RA animals, compared to control in the multivariable model and after adjusting for diet (RA vs Control: β=-4.29, 95%CIs: -8.52, -0.06; p=0.04), whereas the percentage PG (most intense peak assigned to C-OH) to amide I ratio did not present significant differences between the groups (RA vs Control: β=-0.74, 95%CIs: -21.18, 19.69; p=0.94). All other differences with respect to type of diet were not statistically significant (p>0.05) (Table 2).

3.2 Analysis of condylar bone

Figure 4 demonstrates FTIRM spectra from the condylar bone of representative specimens per group. The peaks identified were assigned to amide I (C=O str of NHCO at 1650 cm^{-1}), amide II (N-H b and C-N str of NHCO at 1540 cm^{-1}), C=O str of α-CO_3 and CH_3/CH_2 b (1450 cm^{-1}), C=O str of β-CO_3 and CH_3/CH_2 b, amide III (C-N str and N-H b of NHCO at 1250 cm^{-1}), C=O b (1150 cm^{-1}), P-O str of PO_4 (1024 cm^{-1}) and β-CO_3 str (875 cm^{-1}), where str and b the stretching and bending vibrations respectively. FTIRM peak fitting of the phosphate region (1150-950 cm^{-1}) based on Gaussian deconvolution is represented in Figure 5.

The results of the descriptive statistics for the mineral to matrix ratio (M) are presented in Table 3. The condylar bone did not reveal significant differences among the diseased and the control animals in the multivariable model after adjusting for diet with respect to mineral to matrix ratio (RA vs Control: β=1.22, 95%CIs: -0.44, 2.88; p=0.15). In addition, differential dietary loading did not reveal a significant effect on the M ratio (soft vs hard: β=0.24, 95%CIs: -1.50, 1.98; p=0.79). The results for the acid phosphate content and crystallinity are summarized in Table 3, as well. No statistically significant differences were found between RA and control groups as well, after adjusting for diet for either acid phosphate content (RA vs Control: β=-0.001, 95%CIs: -0.009, 0.008; p=0.84), or crystallinity (RA vs Control: β= 0.05, 95%CIs: -0.09, 0.20; p=0.46). Again, acid phosphate content (soft vs hard: β=0.003, 95%CIs: -0.005, 0.012; p=0.45) and crystallinity (soft vs hard: β=0.07, 95%CIs: -0.07, 0.21; p=0.32) were not influenced from the effect of diet (Table 4).

4. Discussion

In this study, the effects of rheumatoid arthritis and functional loading on the structure configuration of the mandibular condylar cartilage/ bone were examined employing FTIR spectroscopy, a technique widely used for the characterization and analysis of bone and cartilage.[20]

Two surface FTIR techniques were employed: Micro-ATR for the analysis of the outer condylar cartilage surface on intact specimens and reflection FTIR microscopy for the analysis of the condylar bone in sectioned specimens. The results from the FTIR technique revealed evidence of denaturation of the collagen secondary structure in both RA groups, thus leading to rejection of the null hypothesis regarding the effect of rheumatoid arthritis. However, this was not the case for functional loading. Collagen type II and proteoglycan represent the main extracellular matrix components of the condylar cartilage, with collagen forming a triple-helix structure and being responsible for the tissue's mechanical properties.[21] Amide I band, residing between 1700cm^{-1} and 1600cm^{-1} is mainly related to C=O stretching vibration and is the most commonly assessed region in studies of collagen structural integrity.[22]

Spectra deconvolution has revealed an array of Amide I band components. Curve-fitting technique through the 2nd derivative spectra was selected on the basis of decoding the overlapping absorbance bands from raw spectra, offering increased specificity in identifying subpeak attributes to protein secondary structure nature. The relative decrease identified for the a-helix/amide I percentage area ratio in the transgenic animals is presumably associated with denaturation of the a-helix structure. A-helix structure is the most prominent secondary structure in proteins, providing integrity in the collagen backbone through hydrogen bonds between N-H and C=O groups of amino acids.[23] Denaturation is associated with disruption of the hydrogen bonds and unfolding of the collagen backbone into a random unordered peptide shape. Identification of separate bands of increased intensity close to the low frequency region of amide I and within 1601-1593 cm^{-1} and

1612-1606 cm^{-1}, for the RA animals may provide further evidence of denaturation of the collagen helix into unordered and unrecognized structures as a result of the disease.

Deconvolution of spectra within the amide III region showed no differences between the RA and control groups. However, absorption bands in this region appeared complex including collagen components along with PG interferences (S-O of sulfate stretching vibrations).

Previous research on the determination of the PG content of the articular cartilage has identified the region of ~1060cm^{-1} as the most promising for detecting C-O stretching vibrations of the PG matrix within the collagen network,[24,25] while others have attributed the characteristic shoulder at ~1060cm^{-1} to the $v_s(SO_3^-)$ stretching vibrations of the glycosaminoglycans (GAG).[26,27] In the present study, spectra deconvolution in the PG region (1140-900cm^{-1}), failed to identify a single specific peak component related to carbohydrate vibration bands. Variability across specimens was detected with regard to the location of the most intense band peak. Potential degradation of the PG and carbohydrate breakdown might have been masked by simultaneous amide I degradation sequences as a result of the collagen disease. Alternatively, this finding might have been related to minimal amounts of PG destruction from the surface layers of the mandibular condyles.

The results from the analysis of the bone specimens did not reveal evidence of compromised mineral phase of the subchondral bone for the RA groups, as was the case with the apparent collagen derangement detected for the overlying mandibular cartilage. The relative nature of the outcome measure used to quantify the mineral content of the specimens which could have been influenced by a simultaneous fluctuation of the collagen matrix content might pose skepticism on the explanation of the results. Furthermore, the comparable to control mineral-to-matrix (M) ratios achieved by the RA groups may reflect an increased remodeling status of their underlying condylar bone as a result of an internal defense mechanism to counteract the initial and progressive

cartilage and synovial membrane inflammation of the mandibular condyle. In a similar study, a comparison of trauma specimens from osteoporotic femoral bone fractures in women with control subjects has not revealed any differences in the mineral-to-matrix ratios as well ($p=0.11$).[28] Analogous research in tissue specimens of long bones from osteoporosis[29] or experimental arthritis and osteogenesis imperfecta models/patients, using FTIR or Raman spectroscopy are in agreement regarding the non-compromised mineral bone phase in the diseased state.[30,31] It has been suggested that matrix proteoglycans are capable of regulating hydroxyapatite formation and nucleation;[32] apparently, the minimal amounts of PG destruction in all groups as identified in the overlying condylar cartilage in the present study may denote a similar condition taking place in the closely related subcartilage bone. Lastly, a potential limited power of the study to identify small effect size differences between the testing groups due to the relative small sample size cannot be overseen. However, the use of the bootstrap method with 500 replications built-in the regression model for the statistical analysis of the data may have accounted for that.

Owing to the lack of a similar study in the literature on the biochemical properties and structure characterization of the mandibular condyle/cartilage under rheumatoid arthritis and modified functional loading, no direct comparison was possible with findings of other investigations. Thus the absence of effect of functional loading noted on alterations in the collagen structure or the biochemical properties of the mandibular condyle, at least within the period studied, cannot be discussed in detail. In as much, extrapolation of the results of the present study to humans and clinical research may constitute an inherent limitation; however, the selection of the transgenic model over induced arthritis models has postulated significant advantages.[33] The animal models used in this study were human- Tumor Necrosis Factor transgenic mice (hTNF-Tg), carrying a mutation in the 3'- hTNF gene, which resulted in a chronic over-expression of the modified hTNF

mRNA. Following, the transgenic strain developed progressive polyarthritis comparable to human rheumatoid arthritis, with complete phenotypic penetrance and temporomandibular joints symmetrically affected.[19]

5. Conclusion

In conclusion the present study has highlighted the significant role of rheumatoid arthritis on the disruption of the collagen structure of the mandibular condylar cartilage, while there was no evident effect of the disease on the mineral content of the subcartilage bone tissue.

Competing Interests

None declared

Funding

No funding was received for this research

References

1. Chiego DJ Jr. Essentials of oral histology and embryology. A clinical approach, Fourth Edition. Elsevier 2013.

2. Dijkgraaf LC, DeBont LG, Boering G, Liem RS. Structure of the normal synovial membrane of the temporomandibular joint: a review of the literature. *J Oral Maxillofac Surg* 1996;**54**(3):332-8.

3. Werner JA, Tillmann B, Schleicher A. Functional anatomy of the temporomandibular joint. A morphologic study on human autopsy material. *Anatomy and Embryology (Berl)* 1991;**183**(1):89-95.

4. Herring SW. TMJ anatomy and animal models. *J Musculoskelet Neuronal Interact* 2003;**3**(4):391-4.

5. Frost HM. Bone's mechanostat: a 2003 update. *Anat Rec A Discov Mol Cell Evol Biol* 2003;**275**(2):1081–101.

6. Klingenberg CP, Mebus K, Auffray JC. Developmental integration in a complex morphological structure: how distinct are the modules in the mouse mandible? *Evol Dev* 2003;**5**(5):522–31.

7. Boyd RL, Gibbs CN, Mahan PE, Richmond AF, Laskon JL. Temporomandibular joint forces measured at the condyle of Macaca arctoides. *Am J Orthod Dentofacial Orthop* 1990;**97**(6):472-9.

8. Kiliaridis S, Thilander B, Kjellberg H, Topouzelis N, Zafiriadis A. Effect of low masticatory function on condylar growth: a morphometric study in the rat. *Am J Orthod Dentofacial Orthop* 1999;**116**(2):121-5.

9. Papachristou DJ, Papachroni KK, Papavassiliou GA, Pirttiniemi P, Gorgoulis V, Piperi C, et al. Functional alterations in mechanical loading of condylar cartilage induces changes in the bony subcondylar region. *Arch Oral Biol* 2009;**54**(11):1035-45.

10. Viguet-Carrin S, Garnero P, Delmas PD. The role of collagen in bone strength. *Osteoporos Int* 2006;**17**(3):319-36 .

11. Unnanuntana A, Rebolledo BJ, Khair MM, DiCarlo EF, Lane JM. Diseases affecting bone quality: beyond osteoporosis. *Clin Orthop Relat Res* 2011;**469**(8):2194-206.

12. Felsenberg D, Boonen S. The bone quality framework: determinants of bone strength and their interrelationships, and implications for osteoporosis management. *Clin Ther* 2005;**27**(1):1–11.

13. Grabner B, Landis WJ, Roschger P, Rinnerthaler S, Peterlik H, Klaushofer K, et al. Age- and genotype-dependence of bone material properties in the osteogenesis imperfecta murine model (oim). *Bone* 2001;**29**(5):453-7.

14. Goupille P, Fouquet B, Goga D, Cotty P, Valat JP. The temporomandibular joint in rheumatoid arthritis: correlations between clinical and tomographic features. *J Dent* 1993;**21**(3):141-6.

15. Gynther GW, Tronje G, Holmlund AB. Radiographic changes in the temporomandibular joint in patients with generalized osteoarthritis and rheumatoid arthritis. *Oral Surg Oral Med Oral Pathol Oral Radiol Endod* 1996;**81**(5):613-8.

16. Helenius LM, Tervahartiala P, Helenius I, Al-Sukhun J, Kivisaari L, Suuronen R, et al. Clinical, radiographic and MRI findings of the temporomandibular joint in patients with different rheumatic diseases. *International J Oral Maxillofac Surg* 2006;**35**(11):983-9.

17. de Jong Z, Munneke M, Lems WF, Zwinderman AH, Kroon HM, Pauwels EK, et al. Slowing of Bone Loss in Patients With Rheumatoid Arthritis by Long-Term High-Intensity Exercise. *Arthritis Rheum* 2004;**50**(4):1066-76.

18. de Jong Z, Munneke M, Zwinderman AH, Kroon HM, Ronday KH,Lems WF, et al. Long term high intensity exercise and damage of small joints in rheumatoid arthritis. *Ann Rheum Dis* 2004;**63**(11):1399–405.

19. Keffer J, Probert L, Cazlaris H, Georgopoulos S, Kaslaris E, Kioussis D, et al. Transgenic mice expressing human tumour necrosis factor: a predictive genetic model of arthritis. *EMBO J* 1991;**10**(13):4025-4031.

20. Boskey A, Camacho NP. FT-IR imaging of native and tissue-engineered bone and cartilage. *Biomaterials* 2007;**28**(15):2465-78.

21. Xu P, Huang J, Cebe P, Kaplan D. Osteogenesis imperfect collagen-like peptides: self-assembly and mineralization on surfaces. *Biomacromolecules*. 2008;**9**(6):1551-7.

22. Bi X, Li G, Doty SB, Camacho NP. A novel method for determination of collagen orientation in cartilage by Fourier transform infrared imaging spectroscopy (FT-IRIS). *Osteoarthritis Cartilage* 2005;**13**(12):1050-8.

23. Barlow DJ, Thornton JM. Helix geometry in proteins. *J Mol Biol* 1988;**201**(3):601–19.

24. Camacho NP, West P, Torzilli PA, Mendelsohn R. FTIR imaging of collagen and proteoglycan in bovine cartilage. *Biopolymers* 2001;**62**(1):1-8.

25. Rieppo L, Saarakkala S, Närhi T, Holopainen J, Lammi M, Helminen HJ, et al. Quantitative analysis of spatial proteoglycan content in articular cartilage with Fourier transform infrared

imaging spectroscopy: Critical evaluation of analysis methods and specificity of the parameters. *Microsc Res Tech* 2010;**73**(5):503-12.

26. Servaty R, Schiller J, Binder H, Arnold K. Hydration of polymeric components of cartilage- an infrared spectroscopic study on hyaluronic acid and chondroitin sulphate. *Int J Biol Macromol* 2001;**28**(2):121-7.

27. Rieppo L, Saarakkala S, Närhi T, Helminen HJ, Jurvelin JS, Rieppo J. Application of second derivative spectroscopy for increasing molecular specificity of fourier transform infrared spectroscopic imaging of articular cartilage. *Osteorthritis Cartilage* 2012;**20**(5):451-9.

28. McCreadie BR, Morris MD, Chen TC, Sudhaker Rao D, Finney WF, Widjaja E, et al. Bone tissue compositional differences in women with and without osteoporotic fracture. *Bone* 2006;**39**(6):1190–95.

29. Misof BM, Gamsjaeger S, Cohen A, Hofstetter B, Roschger P, Stein E, et al. Bone material properties in premenopausal women with idiopathic osteoporosis. *J Bone Miner Res* 2012;**27**(12):2551-61.

30. Inzana JA, Maher JR, Takahata M, Schwarz EM, Berger AJ, Awad HA. Bone Fragility Beyond Strength and Mineral Density: Raman Spectroscopy Predicts Femoral Fracture Toughness in a Murine Model of Rheumatoid Arthritis. *J Biomech* 2013;**46**(4):723-30.

31. Imbert L, Aurégan JC, Pernelle K, Hoc T. Mechanical and chemical properties of osteogenesis imperfecta human bones at tissue level. *Bone* 2014;***65***:18-24.

32. Boskey AL, Spevak L, Doty SB, Rosenberg L. Effects of bone CS-proteoglycans, DS-decorin, and DS-biglycan on hydroxyapatite formation in a gelatin gel. *Calcif Tissue Int* 1997;**61**(4):298-305.

33. Kannan K, Ortmann RA, Kimpel D. Animal models of rheumatoid arthritis and their relevance to human disease. *Pathophysiology* 2005;**12**(3):167-81.

Figure Captions

Figure 1. Representative ATR-FTIR spectra of the treatment groups (absorbance scale, 2000-650 cm^{-1} region). X-axis represents wavenumbers (cm^{-1}) and y-axis denotes absorption.

Figure 2. ATR-FTIR peak fitting of the amide I region (1750-1550 cm^{-1}) based on the 2nd derivative. X-axis represents wavenumbers (cm^{-1}) and y-axis denotes absorption.

Figure 3. ATR-FTIR peak fitting of the amide III region and PG region (1400-900 cm^{-1}) based on the 2nd derivative. X-axis represents wavenumbers (cm^{-1}) and y-axis denotes absorption.

Figure 4. Representative FTIRM spectra of the treatment groups (absorbance scale, 2000-650 cm^{-1} region). X-axis represents wavenumbers (cm^{-1}) and y-axis denotes absorption.

Figure 5. FTIRM peak fitting of the phosphate region (1150-950 cm^{-1}) based on Gaussian deconvolution. X-axis represents wavenumbers (cm^{-1}) and y-axis denotes absorption.

Table 1. Descriptive statistics for a-helix to amide I and proteoglycan (PG) to amide I ratios of cartilage specimens across groups.

	Control-hard	Control-soft	RA-hard	RA-soft
	a-helix / amide I ratio			
Median	19.82	17.14	15.21	13.59
Interquantile Range (IQR)	12.58	10.77	2.08	1.04
Min-Max	13.97-27.18	14.67-27.45	13.54-25.19	12.43-23.99
	PG / amide I ratio			
Median	50.50	60.00	65.00	53.00
Interquantile Range (IQR)	12.00	50.00	37.00	22.00
Min-Max	33.00-79.00	32.00-100.00	41.00-87.00	34.00-76.00

Table 2. Univariable and multivariable linear regression with observed coefficients in % and 95% confidence Intervals (CIs), for a-helix(1671-1660cm^{-1}) to amide I and PG to amide I ratios. Standard errors (SE) were calculated using the bootstrap method with 500 replications.

	Category	Univariable Analysis			Multivariable Analysis		
		Observed coefficient (β)	**95% CI**	**p-value**	**Observed coefficient (β)**	**95% CI**	**p-value**
a-helix(1671-1660cm^{-1}) to amide I ratios							
Disease	*No (control)*	Reference			Reference		
	Yes (rheumatoid arthritis-RA)	-4.36	-8.42, -0.31	0.03	-4.29	-8.52, -0.06	0.04
Diet	*Hard (standard)*	Reference			Reference		
	Soft	-1.18	-5.95, 3.59	0.63	-0.79	-5.40, 3.82	0.74
Interaction term (disease*diet) is non-significant, p=0.78							
PG to amide I ratios							
Disease	*No (control)*	Reference			Reference		
	Yes (rheumatoid arthritis-RA)	-0.27	-18.44, 17.90	0.98	-0.74	-21.18, 19.69	0.94
Diet	*Hard (standard)*	Reference			Reference		
	Soft	3.14	-15.04, 21.31	0.74	3.24	-17.24, 23.73	0.76
Interaction term (disease*diet) is non-significant, p=0.17							

Table 3. Descriptive statistics for the mineral-to-matrix (M), acid phosphate content and crystallinity of bone specimens across groups.

	Control-hard	Control-soft	RA-hard	RA-soft
	Mineral / matrix ratio (M)			
Median	5.79	5.55	7.74	6.18
Interquantile Range (IQR)	0.78	1.83	0.33	5.35
Min-Max	5.16-6.49	4.13-11.31	6.35-8.02	4.60-10.66
	Acid-phosphate / total phosphate ratio			
Median	0.043	0.051	0.052	0.046
Interquantile Range (IQR)	0.004	0.007	0.004	0.016
Min-Max	0.041-0.049	0.046-0.079	0.046-0.059	0.037-0.058
	Phosphate Crystallinity			
Median	1.88	1.91	1.98	2.03
Interquantile Range (IQR)	0.06	0.11	0.21	0.21
Min-Max	1.78-2.03	1.87-2.08	1.78-2.07	1.60-2.30

T**able 4.** Univariable and multivariable linear regression with observed coefficients in % and 95% confidence Intervals (CIs), for mineral-to-matrix (MM) ratios, acid phosphate content (acid-phosphate/total phosphate ratio) and mineral crystallinity (1030/1020 cm^{-1}) from the subchondral bone region. Standard errors (SE) were calculated using the bootstrap method with 500 replications.

	Category	**Univariable Analysis**			**Multivariable Analysis**		
		Observed coefficient (β)	**95% CI**	**p-value**	**Observed coefficient (β)**	**95% CI**	**p-value**
Mineral to matrix ratios (M)							
Disease	*No (control)*	Reference			Reference		
	Yes (rheumatoid arthritis-RA)	1.22	-0.41, 2.85	0.14	1.22	-0.44, 2.88	0.15
Diet	*Hard (standard)*	Reference			Reference		
	Soft	0.24	-1.55, 2.02	0.80	0.24	-1.50, 1.98	0.79
Interaction term (disease*diet) is non-significant, p=0.65							
Acid phosphate content							
Disease	*No (control)*	Reference			Reference		
	Yes (rheumatoid arthritis-RA)	-0.001	-0.009, 0.007	0.84	-0.001	-0.009, 0.008	0.84
Diet	*Hard (standard)*	Reference			Reference		

	Soft	0.003	-0.005, 0.011	0.42	0.003	-0.005, 0.012	0.45
Interaction term (disease*diet) is non-significant, p=0.06							
Mineral Crystallinity (1030/1020 cm^{-1})							
Disease	*No (control)*	Reference			Reference		
	Yes (rheumatoid arthritis-RA)	0.05	-0.09, 0.19	0.45	0.05	-0.09, 0.20	0.46
Diet	*Hard (standard)*	Reference			Reference		
	Soft	0.07	-0.07, 0.20	0.31	0.07	-0.07, 0.21	0.32
Interaction term (disease*diet) is non-significant, p=0.74							

Figure 1

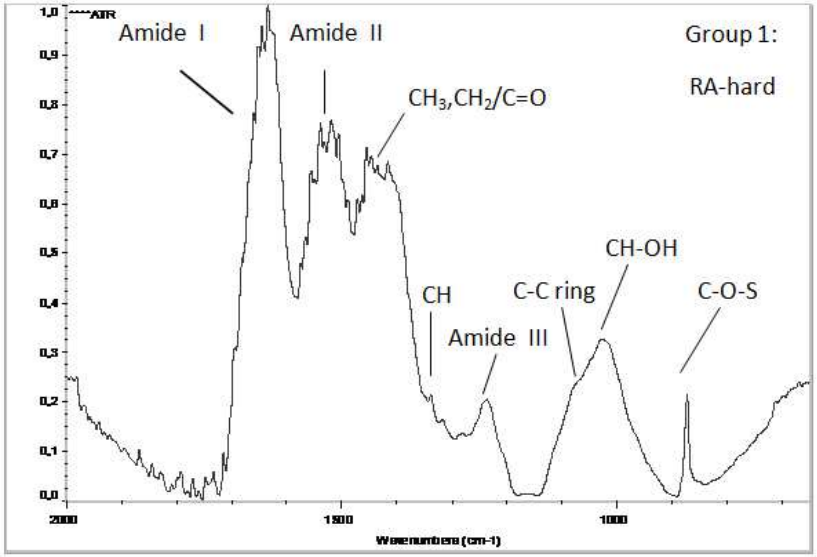
ATR
Amide I
Amide II
CH3,CH2/C=O
CH
Amide III
C-C ring
CH-OH
C-O-S
Group 1:
RA-hard
Wavenumbers (cm-1)

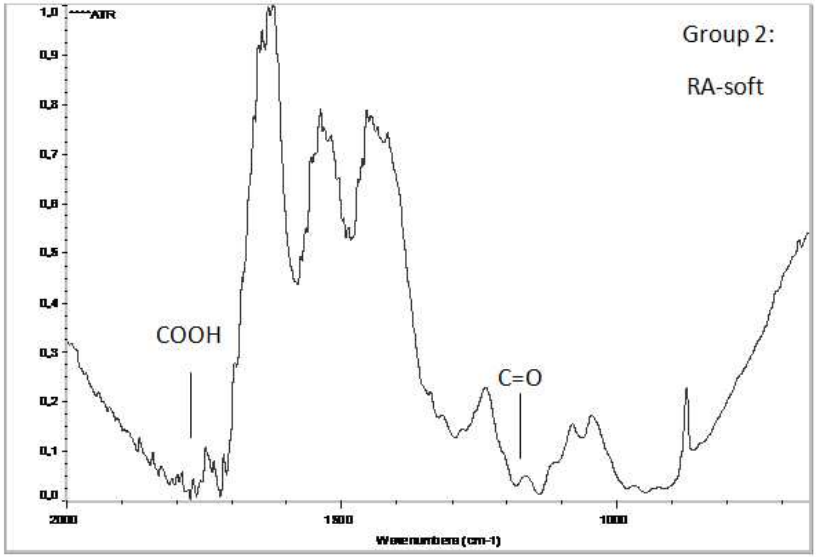
ATR
COOH
C=O
Group 2:
RA-soft
Wavenumbers (cm-1)

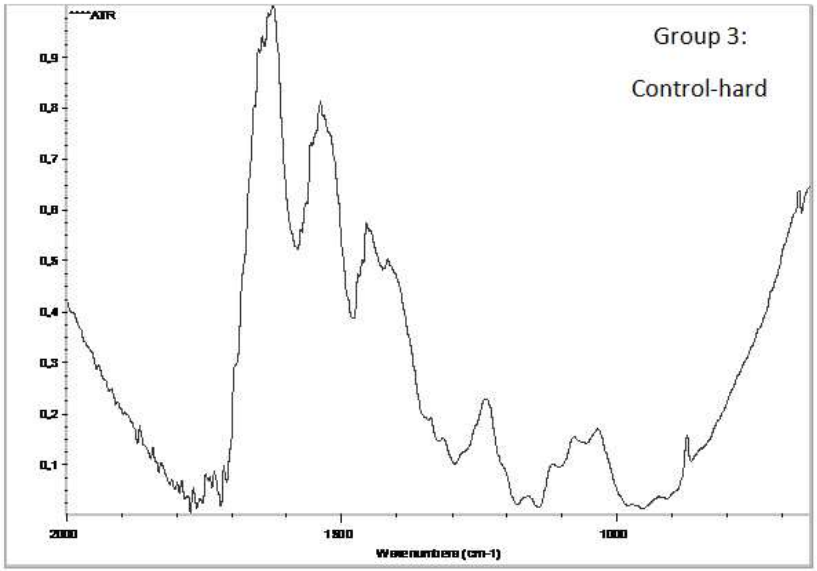
ATR
Group 3:
Control-hard
Wavenumbers (cm-1)

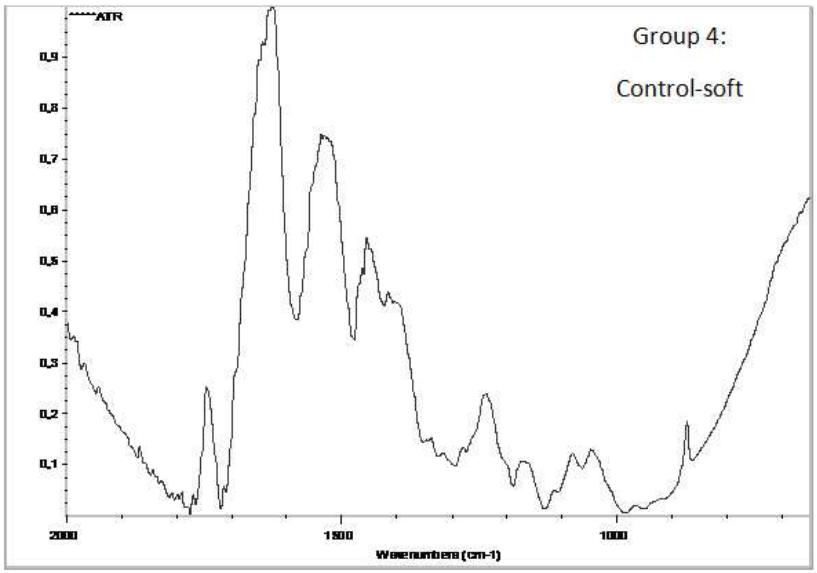
ATR
Group 4:
Control-soft
Wavenumbers (cm-1)

Figure 2

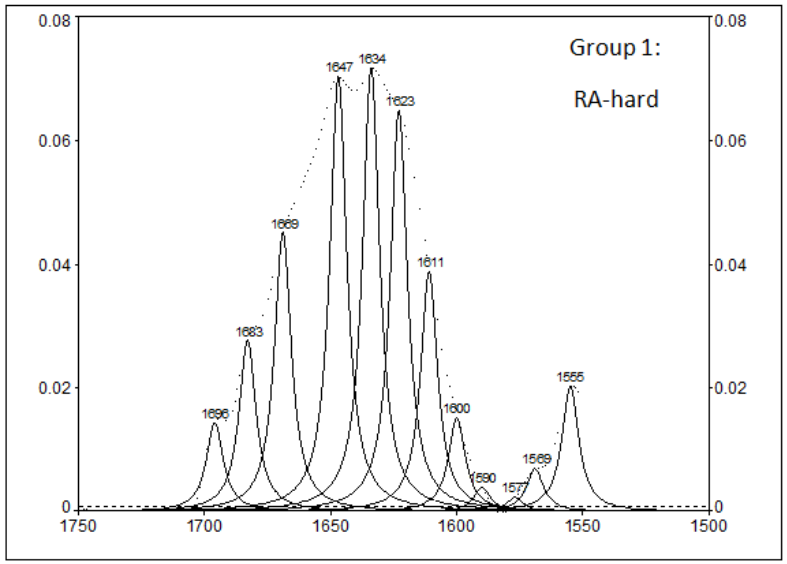
Group 1:
RA-hard
1647
1634
1623
1669
1611
1683
1555
1696
1600
1569
1590
1577
0.08
0.06
0.04
0.02
0
1750
1700
1650
1600
1550
1500

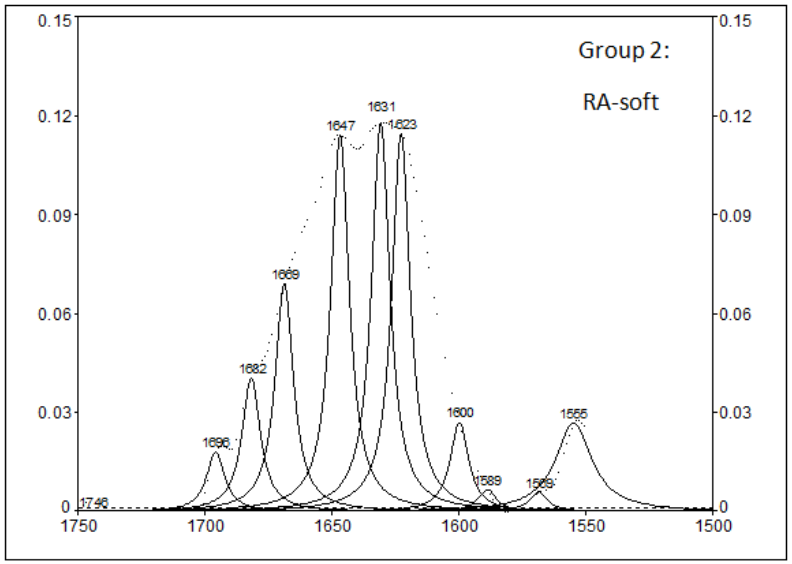
Group 2:
RA-soft
1631
1647
1623
1669
1682
1600
1555
1696
1589
1569
1746
0.15
0.12
0.09
0.06
0.03
0
1750
1700
1650
1600
1550
1500

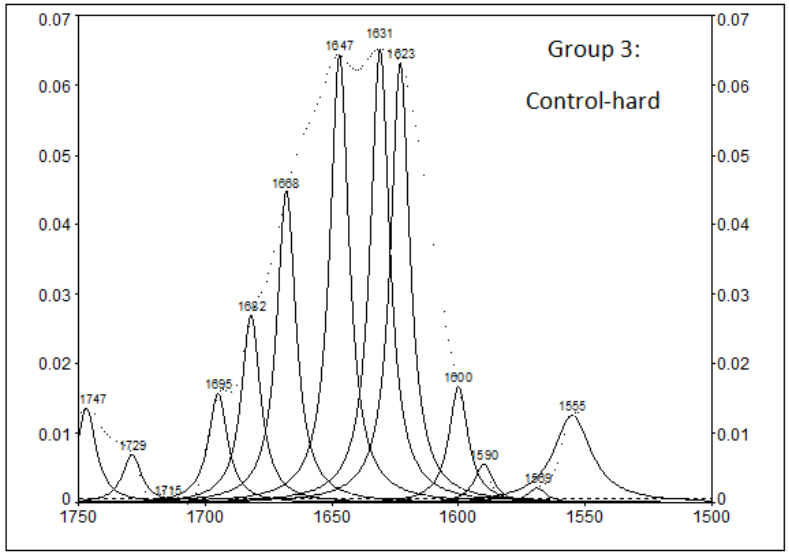
Group 3:
Control-hard
1647
1631
1623
1668
1682
1695
1600
1555
1747
1729
1590
1715
1569
0.07
0.06
0.05
0.04
0.03
0.02
0.01
0
1750
1700
1650
1600
1550
1500

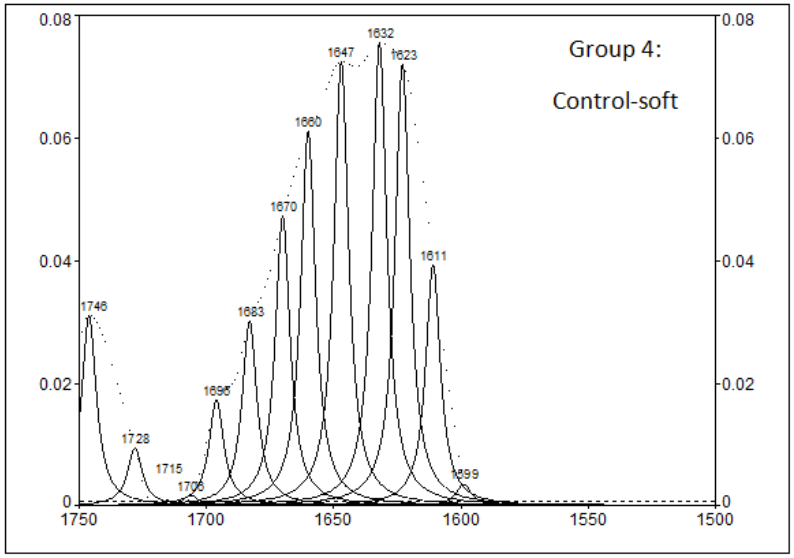
Group 4:
Control-soft
1632
1647
1623
1660
1670
1611
1683
1746
1695
1728
1715
1706
1599
0.08
0.06
0.04
0.02
0
1750
1700
1650
1600
1550
1500

Figure 3

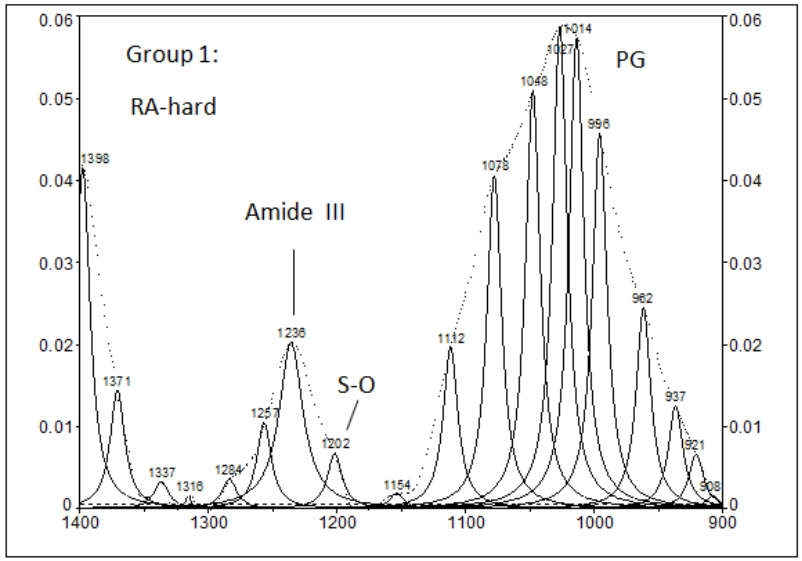
Group 1:
RA-hard
Amide III
S-O
PG
1398
1371
1337
1316
1284
1257
1236
1202
1154
1112
1078
1048
1027
1014
996
962
937
921
908

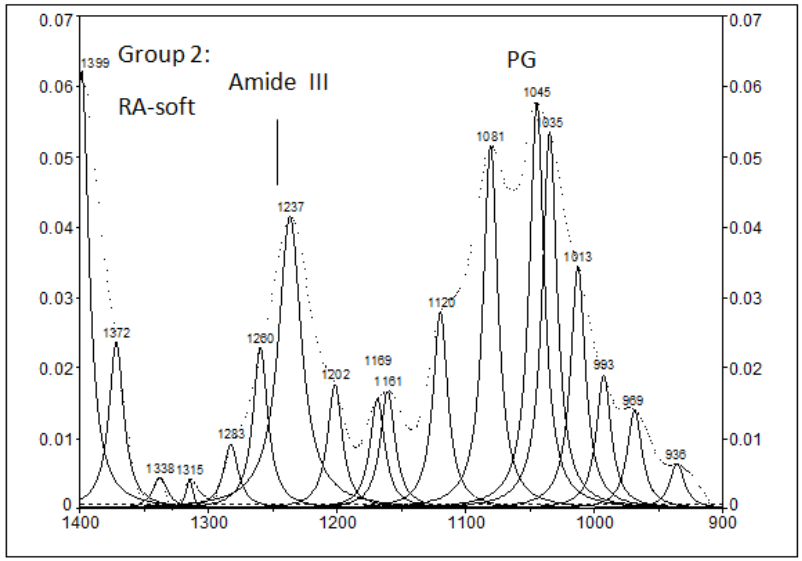
Group 2:
RA-soft
Amide III
PG
1399
1372
1338
1315
1283
1260
1237
1202
1169
1161
1120
1081
1045
1035
1013
993
969
936

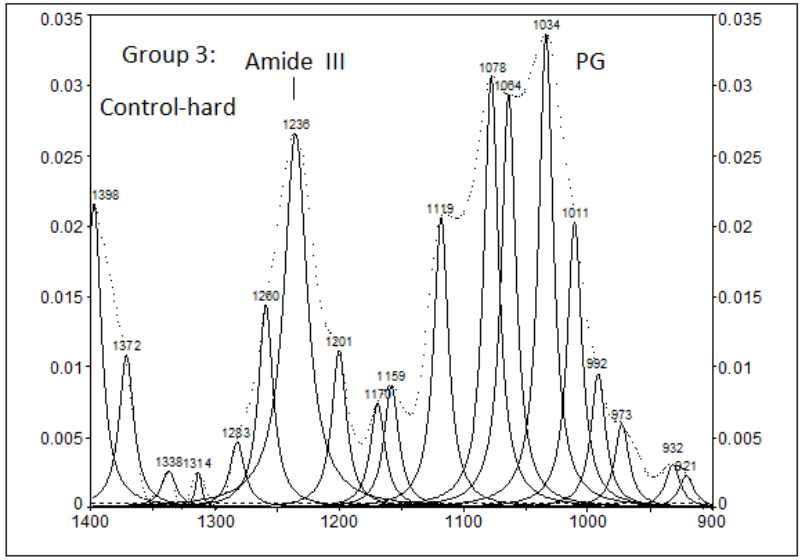
Group 3:
Control-hard
Amide III
PG
1398
1372
1338
1314
1283
1260
1236
1201
1170
1159
1119
1078
1064
1034
1011
992
973
932
921

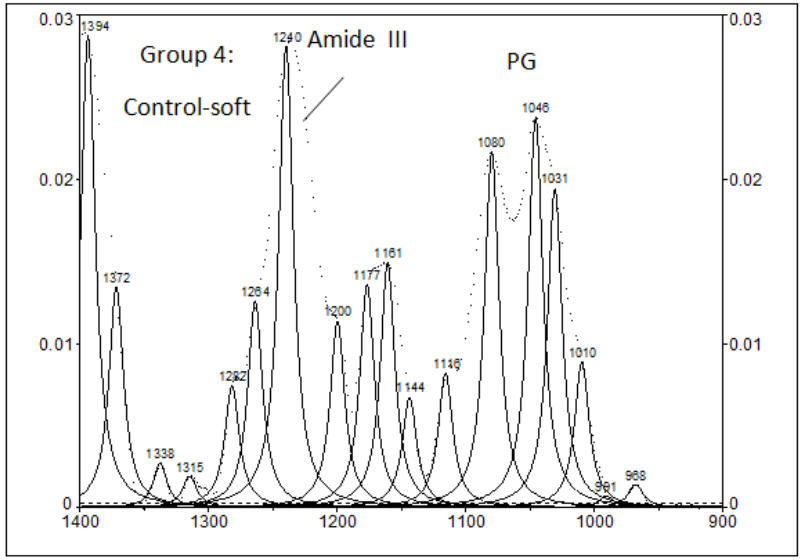
Group 4:
Control-soft
Amide III
PG
1394
1372
1338
1315
1282
1264
1240
1200
1177
1161
1144
1116
1080
1046
1031
1010
981
968

Figure 4

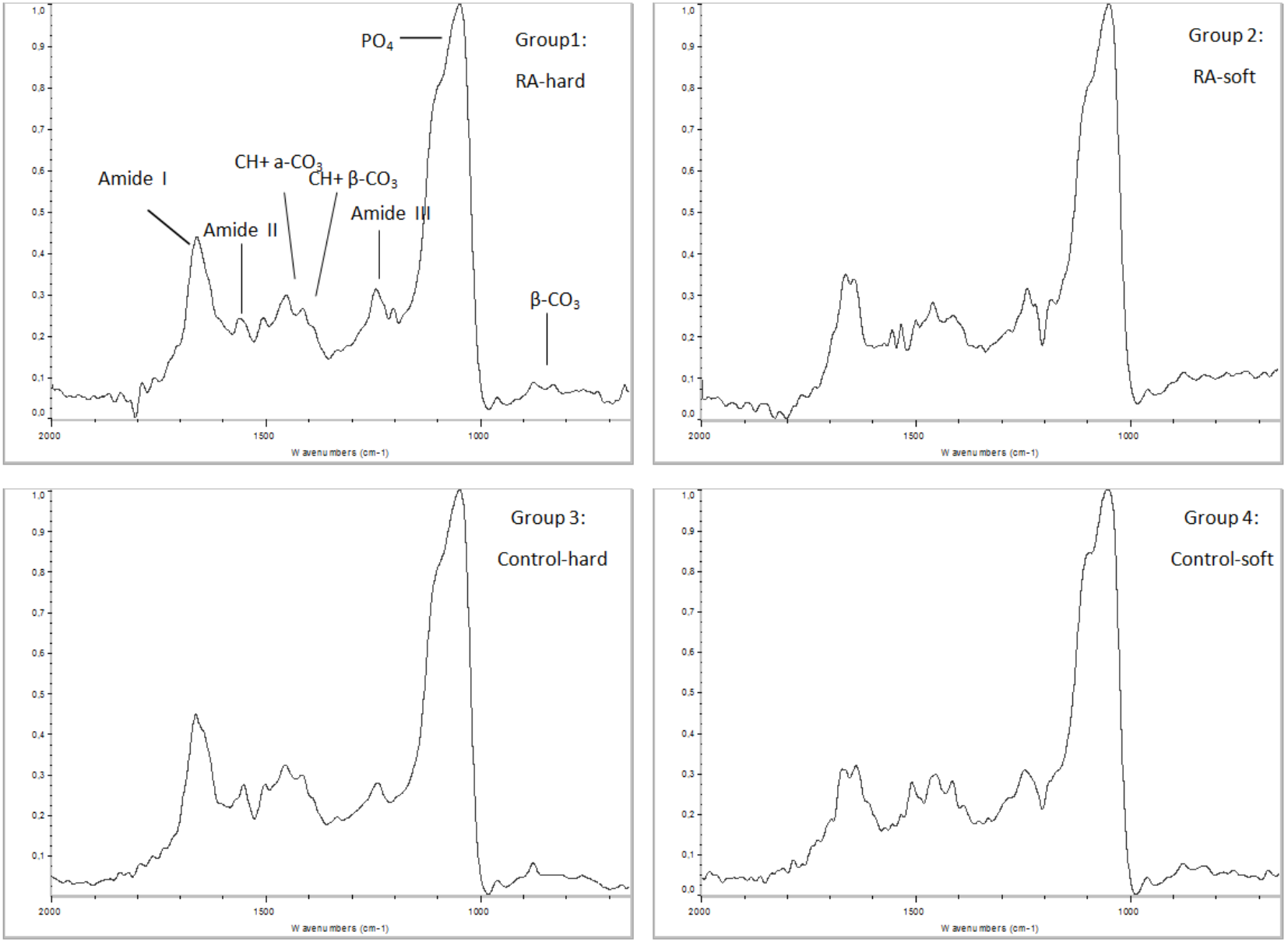
PO4
Group1:
RA-hard
Amide I
CH+ a-CO3
CH+ β-CO3
Amide II
Amide III
β-CO3
Group 2:
RA-soft
Group 3:
Control-hard
Group 4:
Control-soft
W avenumbers (cm-1)

Figure 5

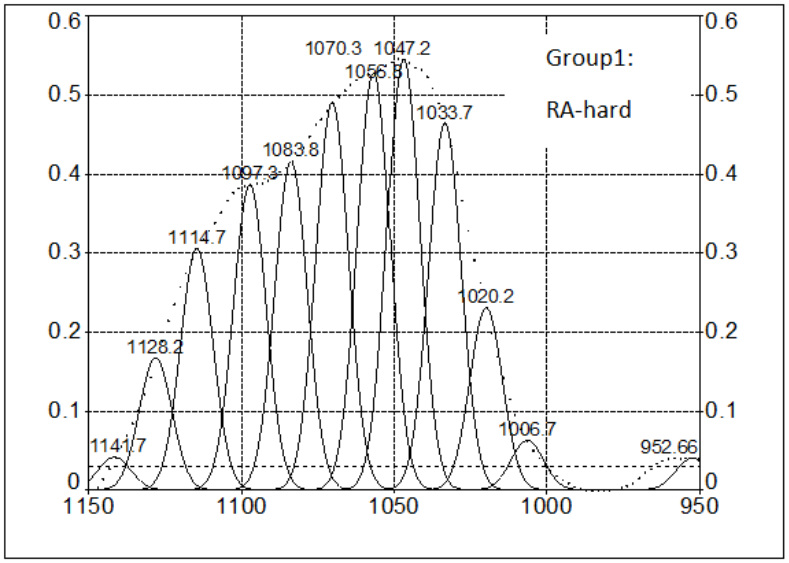
Group1:
RA-hard
1070.3
1047.2
1056.3
1033.7
1083.8
1097.3
1114.7
1020.2
1128.2
1006.7
1141.7
952.66

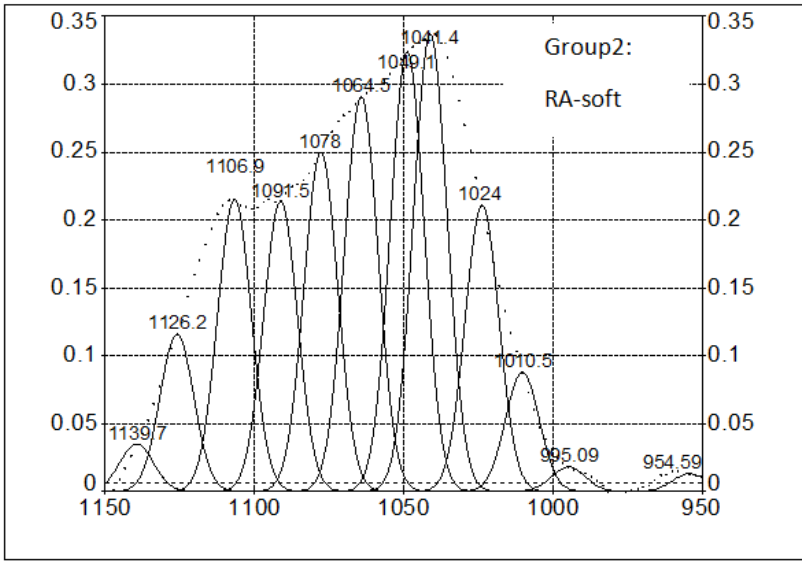
Group2:
RA-soft
1041.4
1039.1
1064.5
1078
1106.9
1091.5
1024
1126.2
1010.5
1139.7
995.09
954.59

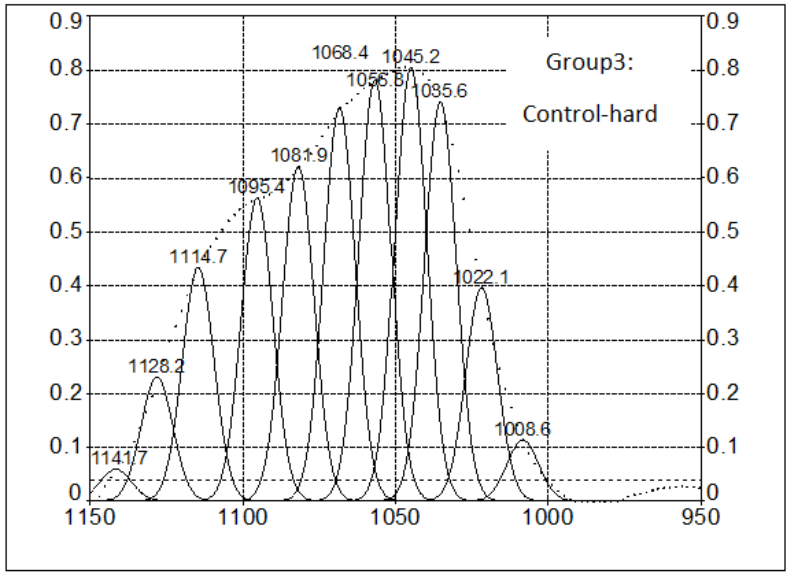
Group3:
Control-hard
1068.4
1045.2
1056.5
1035.6
1081.9
1095.4
1114.7
1022.1
1128.2
1008.6
1141.7

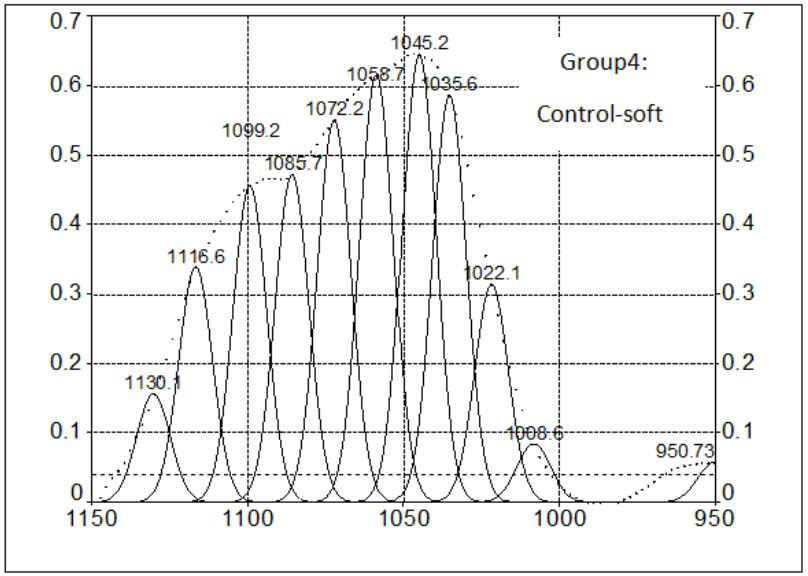
Group4:
Control-soft
1045.2
1058.7
1035.6
1072.2
1099.2
1085.7
1116.6
1022.1
1130.1
1008.6
950.73